Available online at www.sciencedirect.com

SciVerse ScienceDirect

Ceramics International 38 (2012) 5401–5409

CERAMICS INTERNATIONAL

www.elsevier.com/locate/ceramint

Structural and electrical properties of bismuth magnesium tantalate pyrochlores

P.Y. Tan [a], K.B. Tan [a,*], C.C. Khaw [c], Z. Zainal [a], S.K. Chen [b], M.P. Chon [a]

[a] Department of Chemistry, Faculty of Science, Universiti Putra Malaysia, 43400 Serdang, Selangor, Malaysia
[b] Department of Physics, Faculty of Science, Universiti Putra Malaysia, 43400 Serdang, Selangor, Malaysia
[c] Department of Mechanical and Material Engineering, Faculty of Engineering and Science, Universiti Tunku Abdul Rahman, Faculty of Engineering and Science, 53300 Kuala Lumpur, Malaysia

Received 9 February 2012; received in revised form 20 March 2012; accepted 20 March 2012
Available online 29 March 2012

Abstract

The subsolidus cubic pyrochlore phases in the Bi_2O_3–MgO–Ta_2O_5 (BMT) system were prepared with the proposed formula, $Bi_{3+(5/2)x}Mg_{2-x}Ta_{3-(3/2)x}O_{14-x}$ ($0.12 \leq x \leq 0.22$). Replacement of smaller cations, Mg^{2+} and Ta^{5+} by larger Bi^{3+} cations with considerable oxygen non-stoichiometry within structure was proposed. The synthesised samples were confirmed phase pure by X-ray powder diffraction and their refined lattice parameters were in the range of 10.5532(4)–10.5672(9) Å. The grain sizes of the samples determined by SEM analysis were in the range of 0.6–10.60 μm and their average relative densities were more than 80%. Five infrared-active modes were also observed in their FTIR spectra due to their metal–oxygen bonds. The BMT pyrochlores were highly electrical resistive with high dielectric constants, ε' in the range of ~70–85; dielectric losses, tan δ in the order of 10^{-3} at frequency 1 MHz and a negative temperature coefficient of permittivities, TCε' of ~−158 to −328 ppm/°C.

Keywords: C. Dielectric properties; D. Tantalates; Pyrochlores; Ceramics

1. Introduction

Oxide pyrochlores with a general formula of $A_2B_2O_7$ have been studied carefully due to their interesting properties. In general, A and B represent cations at different crystallographic sites as A site is eight-coordinated and B site is six-coordinated with different anions. Due to the compositional variables and structural complexity of pyrochlore phases, two different types of pyrochlore, e.g. $A_2^{2+}B_2^{5+}O_7$ and $A_2^{3+}B_2^{4+}O_7$ or required average mixed valence type are reported. This includes a wide variety of pyrochlores, $Cd_2Nb_2O_7$, $Hg_2V_2O_7$ and $Pb_2Ta_2O_7$ in $A_2^{2+}B_2^{5+}O_7$ system and lanthanide based pyrochlores, $Ln_2Sn_2O_7$ and $Ln_2Pb_2O_7$ in $A_2^{3+}B_2^{4+}O_7$ system. Pyrochlore materials demonstrate a wide spectrum of electrical properties ranging from insulating to metallic of which few compounds exhibiting semiconductor-to-metal transition. The applications of these materials are found in capacitors, thermistors, resistors, switching elements and microwave communication [1].

Recently, Bi-based pyrochlores in the Bi_2O_3–ZnO–X_2O_5 (X = Sb, Ta and Nb) ternary systems have triggered great research interests owing to their relatively low sintering temperatures and excellent dielectric properties [2–4]. Two structurally related compositions, $Bi_3Zn_2Nb_3O_{14}$ (P-phase) and $Bi_4Zn_{4/3}Nb_{8/3}O_{14}$ (β-phase) have been reported in the Bi_2O_3–ZnO–Nb_2O_5 ternary system. The P-phase existed as cubic pyrochlore whereas the β-phase was found as monoclinic zirconolite-phase. $Bi_3Zn_2Nb_3O_{14}$ exhibited a high dielectric constant, $\varepsilon' = \sim 150$ and low dielectric loss, tan $\delta \approx 0.0005$ at 1 MHz, together with a negative temperature coefficient of capacitance, TCC ~−500 ppm/°C. On the other hand, $Bi_4Zn_{4/3}Nb_{8/3}O_{14}$ had slightly lower $\varepsilon' = 80$, tan $\delta = \sim 0.001$, and a positive TCC of +200 ppm/°C at 1 MHz [4–7]. Given the opposite signs of temperature coefficient of capacitance, this gave a strong indication to achieve dielectrics with NPO (negative positive zero) characteristic of 0 ppm/°C if careful composition and processing control were applied [7].

* Corresponding author. Tel.: +60 3 89467491; fax: +60 3 89435380.
E-mail address: tankb@science.upm.edu.my (K.B. Tan).

0272-8842/$36.00
http://dx.doi.org/10.1016/j.ceramint.2012.03.050

In the case of Ta analogue, ideal nominal composition, $Bi_3Zn_2Ta_3O_{14}$ was reported in the Bi_2O_3–ZnO–Ta_2O_5 system as confirmed by detailed phase diagram study [7]. It existed as cubic pyrochlore with ε' of 58, tan δ of 0.0023 at 30 °C and 1 MHz; TCC of −156 ppm/°C in the range of 30–300 °C at 1 MHz [4]. On the other hand, Sb analogue showed extremely low electrical conductivity, $1.00 \times 10^{-20}\ \Omega^{-1}\ cm^{-1}$ at room temperature as determined using extrapolation method [8]. $Bi_3Zn_2Sb_3O_{14}$ showed lower ε' of ∼32 with a tan δ of ∼0.0001 at room temperature, 1 MHz [9]. Among pyrochlores in the Bi_2O_3–ZnO–M_2O_5 (M = Sb, Nb and Ta) ternary systems, lowest ε' in the Sb analogue was postulated to be resulted from the relatively lower polarisability of SbO_6 octahedra within the structure [9,10].

Enormous attempts are made to reduce the dielectric loss and to fine-tune the dielectric constant of dielectric materials, making them suitable candidates for various electrical applications. The low dielectric loss of MgO and comparable ionic radii between Mg^{2+}, 0.72 Å and Zn^{2+}, 0.74 Å have shed new idea to study the Mg-substituted pyrochlore phases [11,12]. There appears limited literature available on pyrochlores in the Bi_2O_3–MgO–Ta_2O_5 (BMT) ternary system and the actual stoichiometry of different phases is still remained unclear. Inconsistencies and controversial descriptions on the pyrochlore phases are found in the two reported different compositions, $Bi_3Mg_2Ta_3O_{14}$ and a bismuth-rich, $Bi_4Mg_{4/3}Ta_{8/3}O_{14}$. Cann et al. [13] reported $Bi_4Mg_{4/3}X_{8/3}O_7$ (X = Ta and Nb) as cubic pyrochlores whereas Sirotinkin and Bush [14] reported Nb analogue, $Bi_3Mg_2Nb_3O_{14}$ existed as single cubic pyrochlore phase. On the other hand, $Bi_3Mg_2Nb_3O_{14}$ was also claimed by Nguyen et al. [15] to contain a trace amount of secondary phase. In this paper, we confirm that none of these compositions exist as phase pure but rather a Bi-rich pyrochlores, $Bi_{3+(5/2)x}Mg_{2-x}Ta_{3-(3/2)x}O_{14-x}$ $(0.12 \leq x \leq 0.22)$ are successfully prepared after firing at the temperature 1025 °C over a duration of 48 h. We also discuss on the structural and electrical properties of BMT pyrochlores using various spectroscopy techniques.

2. Experimental

Samples of nominal compositions, $Bi_3Mg_2Ta_3O_{14}$, $Bi_4Mg_{4/3}Ta_{8/3}O_{14}$ and $Bi_{3+(5/2)x}Mg_{2-x}Ta_{3-(3/2)x}O_{14-x}$ (x = 0.12, 0.14, 0.16, 0.18, 0.20, 0.22) were prepared by conventional solid state method. The starting materials were reagent grade oxide powders, Bi_2O_3 (Alfa Aesar, 99.99%), MgO (Aldrich, 99%) and Ta_2O_5 (Alfa Aesar, 99.9%). Stoichiometric amount of oxides were weighed and mixed homogeneously with acetone in an agate mortar. The mixed powders were then transferred into the platinum boat for calcinations. The samples were pre-treated at 300 °C for 1 h and further heated at 600 °C for 1 h to ensure the Bi_2O_3 reacted to form less-volatile compounds; this allowed firing at higher temperatures without significant losses of bismuth. The pre-treated powders were heated at 800 °C overnight and further synthesised at 1025 °C for 48 h with intermediate regrinding to reach equilibrium. The powders were pressed into pellets of 8 mm in diameter and ∼1.5 mm in thickness prior to sintering at 1075 °C for 24 h.

The phase purity of the samples were characterised by X-ray powder diffraction using an automated Shimadzu diffractometer XRD 6000, Cu Kα radiation in 2θ range of 10–70° at the scan speed of 2°/min. Data for lattice parameter determination were collected at a scan rate of 0.1°/min and the refinement was performed by *Chekcell* software. The relative densities were also calculated from comparisons of densities which determined by both geometrically and theoretically. The surface morphologies of the samples were examined by scanning electron microscopy (SEM, JOEL JSM-6400). The elemental analysis was conducted by ICP-OES, Perkin Elmer Optima 2000DV using triplicate samples.

The electrical behaviours of the samples were measured using HP4192A ac impedance analyser in the frequency range of 5 Hz–13 MHz. Gold coated pellet was attached to conductivity jig prior to electrical measurement in temperature controlled horizontal tube furnace. The electrical data were collected in heat–cool cycle in the temperature range of 30–850 °C after 25 min equilibration time.

3. Results and discussion

3.1. XRD and elemental analysis

Fig. 1a and b shows the XRD patterns for the nominal compositions $Bi_3Mg_2Ta_3O_{14}$, P (x = 0) and $Bi_4Mg_{4/3}Ta_{8/3}O_{14}$ which synthesised at 1025 °C. In Fig. 1a, additional diffraction planes observed at 2θ, 19.8800° and 32.4059° are attributed to $Mg_4Ta_2O_9$ (ICDD 38-1458). Meanwhile, the reported $Bi_4Mg_{4/3}Ta_{8/3}O_{14}$ is found to be mixed phases of monoclinic and cubic phases. Our observation disagrees to those results in literature [13–15]. The phase pure cubic pyrochlore phases in Bi_2O_3–MgO–Ta_2O_5 system are formed with the proposed formula, $Bi_{3+(5/2)x}Mg_{2-x}Ta_{3-(3/2)x}O_{14-x}$ $(0.12 \leq x \leq 0.22)$ as evidently shown in Fig. 1c. All characteristic peaks belonging to cubic pyrochlore are fully indexed based on space group, *Fd*3*m*. On the other hand, Fig. 2 shows the partial subsolidus phase diagram of Bi_2O_3–MgO–Ta_2O_5 system, which includes the ideal P and solid solution series. The phase pure samples are deviated away from ideal P, composition, having richer bismuth in content, e.g. 41 mol% above. The three different types of metal ions in the samples vary with x for which increase of Bi is compensated by a decrease of Mg and Ta cations together with a variation of oxygen within the structure. The locus of the solid solution behaves towards direction of Bi_2O_3 as denoted in the cations ratio, Bi: Mg: Ta is 5/2: 1: 3/2.

Fig. 3 shows the variation of lattice parameters as a function of composition. The lattice parameters for the samples are in the range of 10.5532 (4)–10.5672 (9) Å. A linear graph with positive gradient is obtained for which the Vegard's law is obeyed. The lattice parameters of a continuous substitutional solid solution should vary linearly with concentration at constant temperature if the chemical bondings of constituent

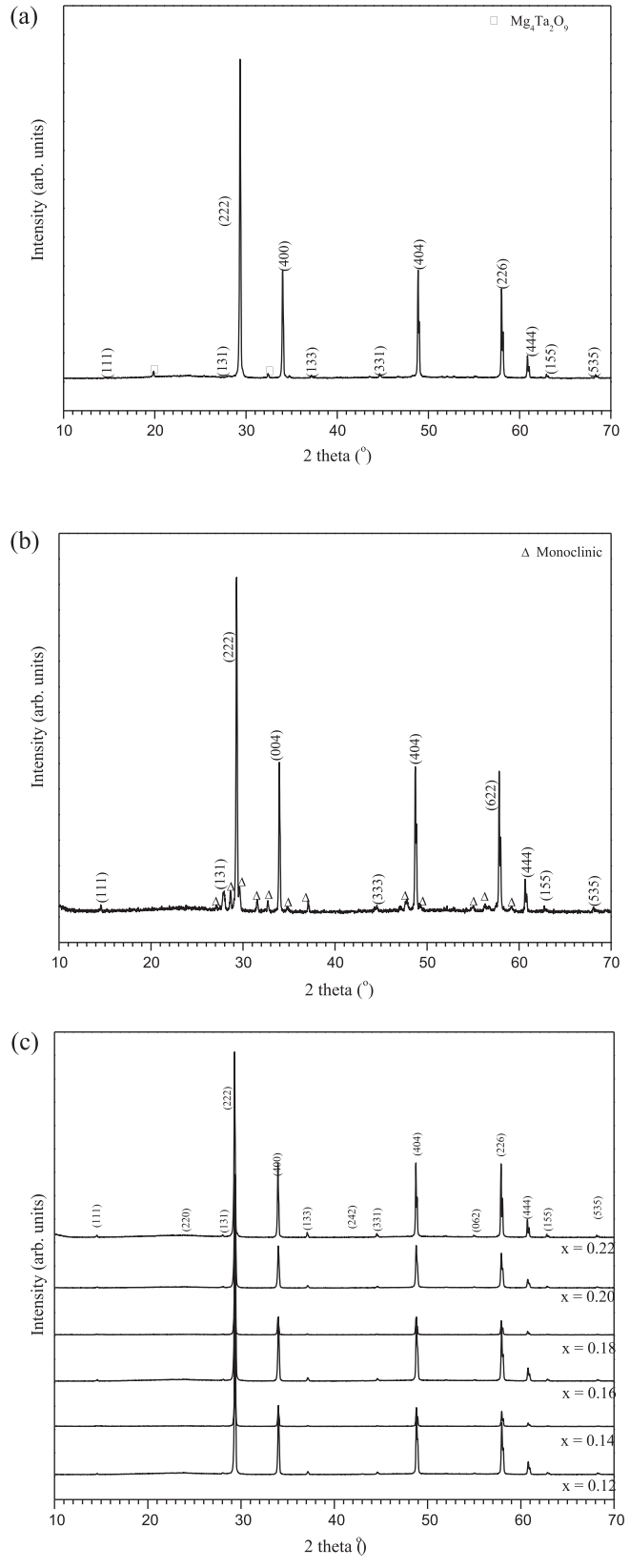

Fig. 1. XRD patterns of prepared samples in the Bi_2O_3–MgO–Ta_2O_5 ternary system. (a) $Bi_3Mg_2Ta_3O_{14}$, (b) $Bi_2Mg_{2/3}Ta_{4/3}O_7$, (c) $Bi_{3+(5/2)x}Mg_{2-x}Ta_{3-(3/2)x}O_{14-x}$ ($0.12 \leq x \leq 0.22$).

phases are similar [16]. Meanwhile, the question immediately arises in the formation mechanism as the compositional variables involving redistribution of the three cations of different sizes at different coordination environments. At the outset, the valence state of cations are assumed to be Bi^{3+}, Mg^{2+} and Ta^{5+}, respectively for which they are coordinated to two different oxygen under a interpenetrating networks consisting of AO_6O_2' and BO_6 polyhedra [17]. Hence, it is presumed that the cation ratios on the A- and B-sites of this average mixed valence $A^{3+}B^{4+}O_6O'$ pyrochlore are set to values consistent with the commonly reported bismuth based pyrochlore analogues $(Bi_3Zn)(ZnM_3)O_{14}$ (M = Sb, Nb and Ta). In this case, Mg cation is expected to be distributed unequally over two different A and B sites. The rationales behind are Mg is more comfortable in a 6 fold coordinated B-site instead of a 8 fold coordinated A-site and also more vacant A sites are required for additional larger Bi [17–20]. However, the A site shall not only be occupied by Bi cations in which the coupling effect of Bi $6s^2$ lone pair may cause cell distortion, leading to formation of monoclinic zirconolite phase [21]. On the other hand, incorporation of higher Bi content has contributed to an expansion of unit cell due to the size factor, i.e. larger ionic radii of Bi^{3+}, 1.17 Å if compared to that of Mg^{2+}, 0.89 Å [12]. The total number of cations and electroneutrality of the subsolidus system are preserved as suggested by the mechanism below:

$$5/2\,Bi^{3+} \leftrightarrow Mg^{2+} + 3/2\ - Ta^{5+} + O^{2-}$$

Table 1 shows the elemental concentrations for the prepared $Bi_{3+(5/2)x}Mg_{2x}Ta_{3-(3/2)x}O_{14-x}$ ($0.12 \leq x \leq 0.22$) samples in terms of atomic%. The percentage of O is obtained by the difference of cations. The results are in good agreement to those calculated values, confirming the stoichiometric compositions of the prepared samples.

3.2. Structure and microstructure

The mean crystallite size, C_{size}, of each of the samples is determined by the Scherrer equation as follow:

$$C_{size} = \frac{k \times \lambda}{\beta \times \cos\theta} \tag{1}$$

where k is a constant, 0.9, λ is the wavelength, β is the full width at half maximum, FWHM of the peak, and θ is the angular position of the peak [2]. These samples have the crystallite sizes in the range of 57–78 nm. The crystallite size and strain-induced broadening of the samples are also determined with Williamson and Hall analysis, which is given by:

$$\frac{\beta\cos\theta}{\lambda} = \frac{0.9}{d_{avg}} + \frac{4\varepsilon\sin\theta}{\lambda} \tag{2}$$

where 0.9 is the shape factor, λ is the $CuK_{\alpha 1}$ radiation of wavelength (λ = 1.5418 Å), β is the FWHM, ε is the strain, and θ is the scattering angle [22,23]. The value of internal strain is obtained from the slope of the graph while the intercept at y-axis gives the inverse of average particle size (Fig. 4). The

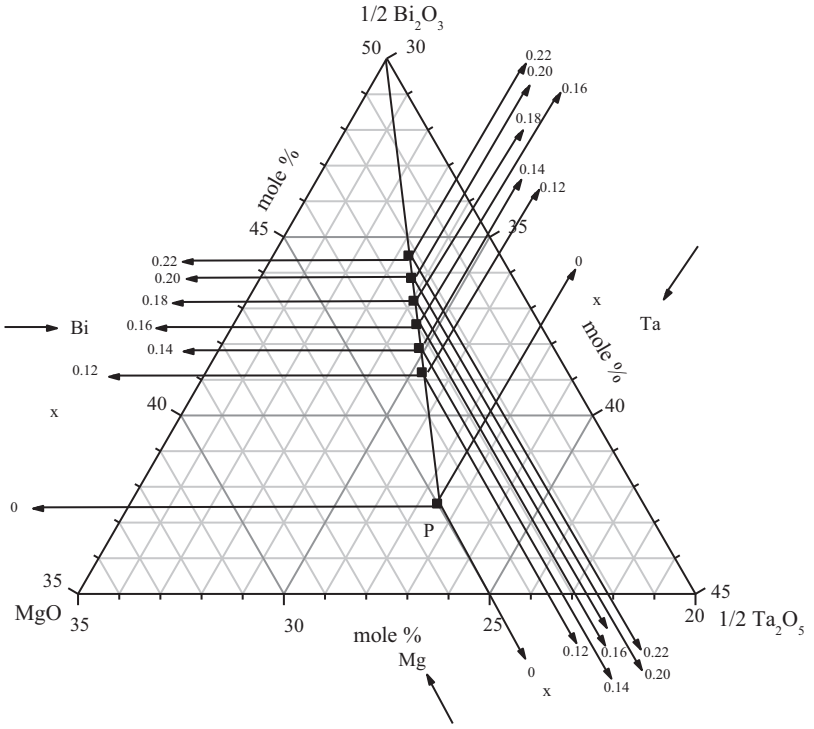

Fig. 2. Expanded Bi_2O_3–MgO–Ta_2O_5 ternary phase diagram in which $Bi_{3+(5/2)x}Mg_{2-x}Ta_{3-(3/2)x}O_{14-x}$ ($0.12 \leq x \leq 0.22$) subsolidus solution is located.

crystallite sizes measured using W–H methods are in the range of 38–53 nm. Small variation of crystallite size is observed and this may resulted from the numbers of peak picked. The calculated strain ε associated with lattice dislocation is found to be very small and negligible, i.e. in the order of 10^{-4}. This implies that increase of Bi content has not resulted in any significant structural deformation of the cubic pyrochlore due to the reason mentioned earlier. The grain sizes of the samples determined from the SEM micrographs, Fig. 5(a)–(f), have the average grain size of 0.6–10.6 μm. These samples are dense and of irregular grains with average relative densities >80% after fired at 1075 °C for 24 h. The grain sizes of the samples are much larger than their crystallite sizes as a grain contains several crystallites. The differences of grain sizes, internal strain and calculated crystallite sizes are summarised in Table 2.

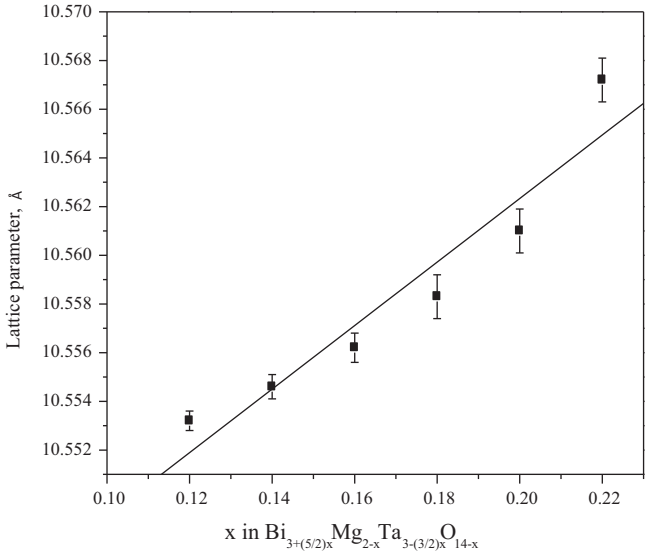

Fig. 3. Variation of lattice parameters as a function of x in the $Bi_{3+(5/2)x}Mg_{2-x}Ta_{3-(3/2)x}O_{14-x}$ ($0.12 \leq x \leq 0.22$) samples.

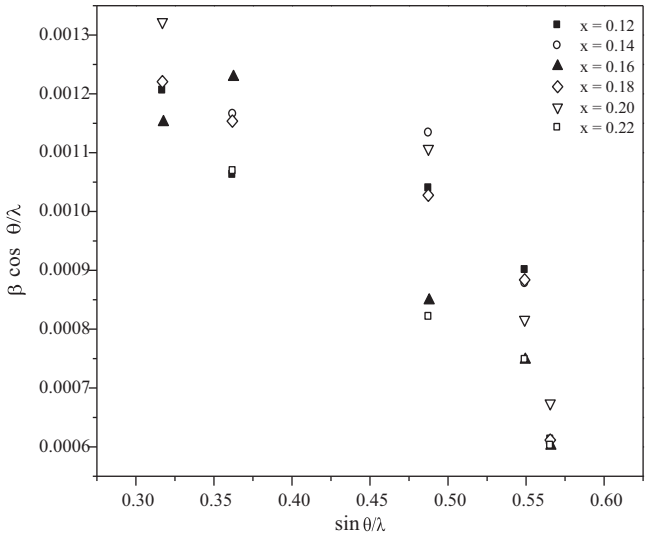

Fig. 4. Williamson–Hall plot of the $Bi_{3+(5/2)x}Mg_{2-x}Ta_{3-(3/2)x}O_{14-x}$ ($0.12 \leq x \leq 0.22$) samples.

Table 1
Elemental concentrations of $Bi_{3+(5/2)x}Mg_{2-x}Ta_{3-(3/2)x}O_{14-x}$ ($x = 0.12$–0.22) solid solution.

Samples	x	Element	Atomic %	
			Calculated	Experimental
$Bi_{3.30}Mg_{1.88}Ta_{2.82}O_{13.88}$	0.12	Bi	46.99	46.45 ± 0.24
		Mg	3.11	3.32 ± 0.04
		Ta	34.77	33.10 ± 0.14
		O	15.13	17.13
$Bi_{3.35}Mg_{1.86}Ta_{2.79}O_{13.86}$	0.14	Bi	47.56	46.97 ± 0.20
		Mg	3.07	3.31 ± 0.03
		Ta	34.3	32.29 ± 0.21
		O	15.07	17.44
$Bi_{3.40}Mg_{1.84}Ta_{2.76}O_{13.84}$	0.16	Bi	48.14	47.75 ± 0.32
		Mg	3.03	3.36 ± 0.02
		Ta	33.83	32.10 ± 0.15
		O	15.00	16.79
$Bi_{3.45}Mg_{1.82}Ta_{2.73}O_{13.82}$	0.18	Bi	48.70	48.70 ± 0.14
		Mg	2.99	3.36 ± 0.01
		Ta	33.37	32.39 ± 0.20
		O	14.94	15.55
$Bi_{3.50}Mg_{1.80}Ta_{2.70}O_{13.80}$	0.20	Bi	49.27	48.77 ± 0.43
		Mg	2.95	3.32 ± 0.02
		Ta	32.91	32.17 ± 0.19
		O	14.87	15.74
$Bi_{3.55}Mg_{1.78}Ta_{2.67}O_{13.78}$	0.22	Bi	49.75	47.36 ± 0.09
		Mg	2.90	3.14 ± 0.02
		Ta	32.40	31.85 ± 0.08
		O	14.95	17.65

3.3. IR spectroscopy

Fig. 6 shows the IR spectra of pyrochlore oxides. The region of interest in IR absorption bands of inorganic compounds are usually in the range of 100–1000 cm^{-1} which attributed to the vibrations of ions in the crystal lattice [10,24,25]. Infrared-active phonon modes have been assigned to specific bending and stretching vibrational modes, which originated from vibration and bending of metal–oxygen bond.

The vibration of the shorter A–O′ bond may correspond to the phonon mode, ω_n** at around 870 cm^{-1} and the vibration of the longer bond may lead to a phonon mode, ω_2 at around 490 cm^{-1}. The disorder of A and O′ ions may due to the static displacements in all pyrochlores in which the Bi cation has active lone pair of $6s^2$ electrons. The displacements of both the O′ anion and the A-site cation must be cooperative within domains and this may lead to the one A–O′ bond being shortened and the other being lengthened [25].

The band in the region 560–770 cm^{-1} can be ascribed to B–O stretching vibration. The two-phonon modes around 566 cm^{-1}, ω_1* and 635 cm^{-1}, ω_1 are very close to each other but not well separated in the spectra. However, the assignment of the internal octahedral modes is based on the bonding character between B and O ions. The stretching vibration frequency of the bond is higher generally for bonding atoms with lighter mass. Hence, the phonon mode at 560 cm^{-1} is assigned to Ta–O while the phonon mode at 630 cm^{-1} is assigned to Mg–O [25]. The phonon modes of BMT pyrochlores are summarised in Table 3.

Table 2
The grain size, crystallites size and the calculated internal strain of $Bi_{3+(5/2)x}Mg_{2-x}Ta_{3-(3/2)x}O_{14-x}$ ($x = 0.12$–0.22) solid solution.

x	C_{size} = average crystallite size		W–H plot, strain	Grain size, μm
	Scherrer (nm)	W–H method (nm)		
0.12	75	53	0.00043	0.60–5.67
0.14	66	43	0.00058	1.33–6.67
0.16	78	45	0.00058	1.50–6.67
0.18	74	47	0.00050	1.17–6.17
0.20	68	41	0.00065	2.50–10.00
0.22	57	38	0.00080	1.40–10.60

3.4. Electrical properties

Complex impedance plots of $Bi_{3.55}Mg_{1.78}Ta_{2.67}O_{13.78}$ are shown in Fig. 7. The impedance data are normalised by geometric factor and corrected for stray capacitance of empty jig. Perfect semicircles are discernable for measurements taken at temperature range of 550–700 °C and the associated capacitances are in the order of 10^{-12} F cm^{-1}, which is typical response of bulk dielectric material [4]. No sign of electrode effects at the low frequency region and no grain boundary effect are observed from the Cole–Cole plots. Therefore, the conducting species are probably attributed to electrons [4]. The electrical data are well represented by parallel RC circuit as shown in inset of Fig. 7 whereby R_b and C_b are bulk resistance and capacitance, respectively. The combined spectroscopic plots of $Bi_{3.55}Mg_{1.78}Ta_{2.67}O_{13.78}$ at 598 °C show FWHM of the M'' peak is approximately 1.22 decade which is close to the perfect Debye (1.14) showing the material is electrically homogenous (Fig. 8).

The Arrhenius conductivity plots of the prepared samples are based on the Arrhenius's law with the expression, $\sigma = \sigma_0 \exp(-E_a/kT)$ where σ_0 is the pre-exponential factor, E_a is the apparent activation of the conduction process, k is Boltzmann's constant and T is the absolute temperature [24]. All the samples have a linear behaviour with activation energies ranging from 1.17 to 1.49 eV. The activation energies for these samples are comparable to $Bi_3Zn_2Sb_3O_{14}$ (1.36 eV), $Bi_3Zn_2Nb_3O_{14}$ (~1.59 eV) and $Bi_3Zn_2Ta_3O_{14}$ (1.55 eV). Consider high activation energy, e.g. >1.0 eV is obtained and this high value usually associated with hopping type of electronic transport mechanism if it is not linked to ionic conduction.

Fig. 9 shows the imaginary part of impedance as a function of frequency on a logarithmic scale for $Bi_{3.55}Mg_{1.78}Ta_{2.67}O_{13.78}$. The presence of a maximum indicates the presence of a polarisation process. The displacement of the maxima of the curves to higher frequencies with the increase in measuring temperature is discernable. The frequency at the maximum value of each peak was plotted as an Arrhenius type of plot to represent its dependence on the temperature. The activation energy, E_a, obtained from the plot is 1.37 eV which is well agreed with the

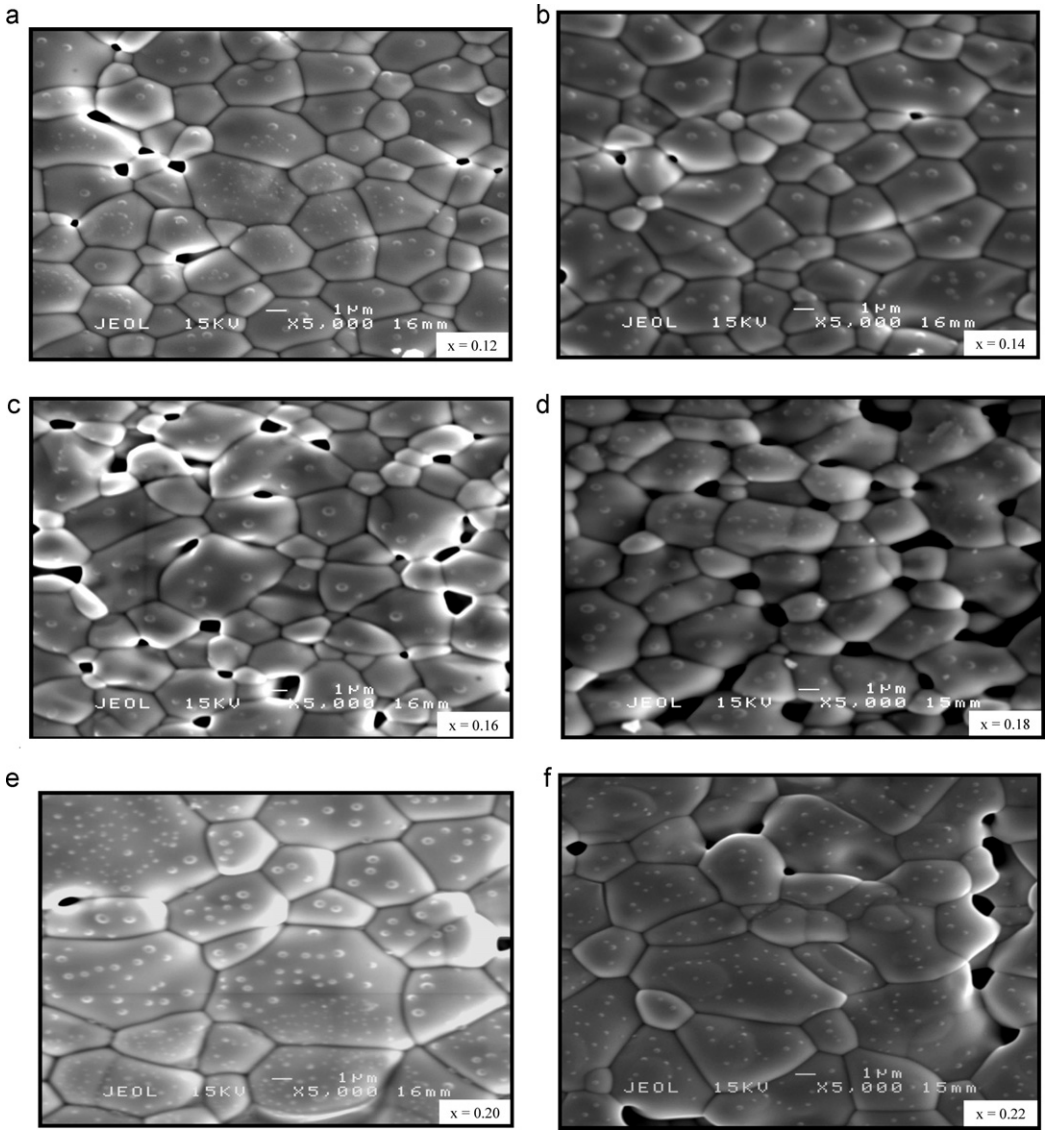

Fig. 5. The SEM micrographs of the $Bi_{3+(5/2)x}Mg_{2-x}Ta_{3-(3/2)x}O_{14-x}$ ($0.12 \leq x \leq 0.22$) samples.

value that obtained from the Arrhenius conductivity plot, E_a = 1.47 eV (Fig. 10). The close agreement between these two values denotes that the polarisation phenomenon of the crystalline lattice has a strong influence on the electrical behaviour, providing additional evidence that the conduction mechanism is of the hopping type [4] (Fig. 11).

Figs. 12 and 13 show the temperature dependence of the dielectric constant, ε' and dielectric loss, tan δ of the prepared

Table 3
The Fourier transform infrared spectra of $Bi_{3+(5/2)x}Mg_{2-x}Ta_{3-(3/2)x}O_{14-x}$ (x = 0.12–0.22) cubic pyrochlores.

Mode	Mode assignment	x					
		0.12	0.14	0.16	0.18	0.20	0.22
		Wavenumber, cm^{-1}					
ω_n**	(A–O′)	874	874	872	872	871	868
	(B–O)	–	767	745	–	–	747
ω_1	(B–O)	645	642	636	646	631	635
ω_1*	(B–O)	566	569	569	570	571	567
ω_2	(A–O′)	492	492	492	494	491	490
ω_3	(A–O)	321	303	303	–	314	304

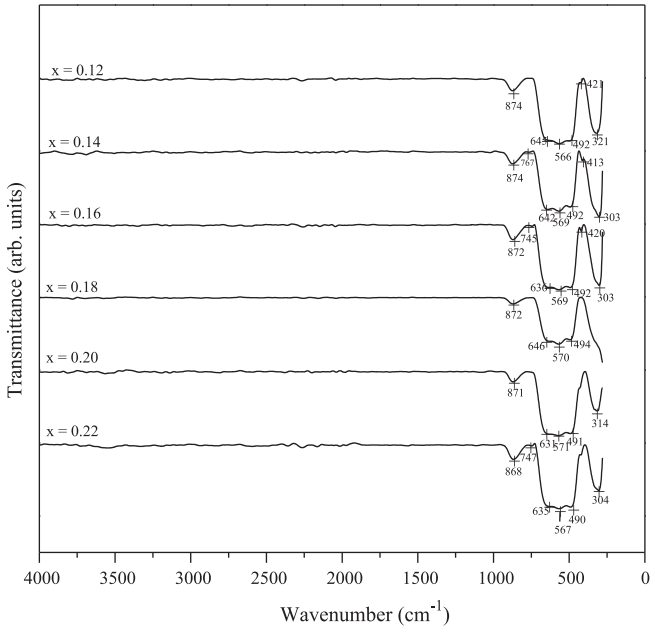

Fig. 6. The FT-IR spectra for the $Bi_{3+(5/2)x}Mg_{2-x}Ta_{3-(3/2)x}O_{14-x}$ ($0.12 \leq x \leq 0.22$) samples.

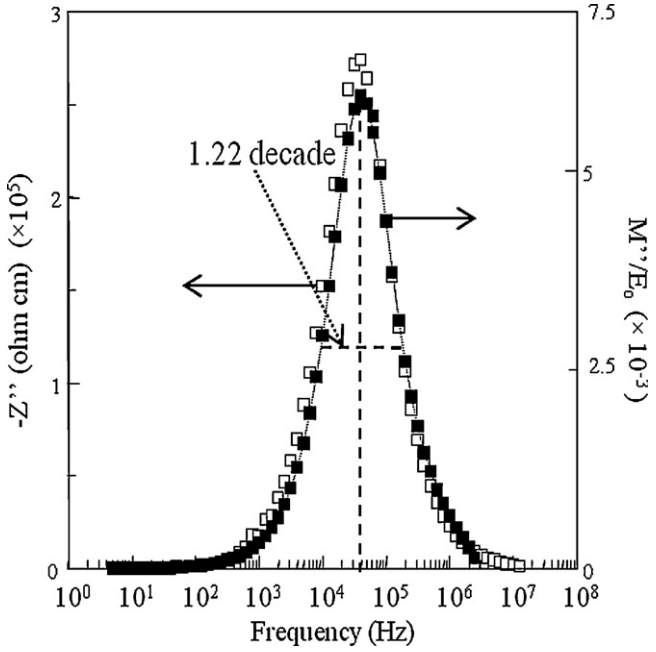

Fig. 8. Combine spectroscopic plots of $Bi_{3.55}Mg_{1.78}Ta_{2.67}O_{13.78}$ at 598 °C.

samples at 1 MHz. The ε' is almost constant with the increase of temperature. Meanwhile, tan δ increases with the increase of temperature above 550 °C. Normally, the temperature dependence of ε' and tan δ may due to the polarisation effect. The number of space–charge carriers that control the space–charge polarisation increases as the temperature increases. This has caused stronger polarisation particularly in dielectric materials [4,10,24,26–29]. These samples measured at room temperature, 1 MHz have the ε' in the range of 73–84 and tan δ values in the order of 10^{-3}. Negative temperature coefficient of permittivity, $TC\varepsilon'$ in the range of −158 to −328 ppm/°C is recorded at 1 MHz in the range of ∼30–300 °C.

The ε' of samples generally increases with the increase of x-value, which corresponds to higher Bi content. In general, the ε' of materials is contributed by the dielectric polarisation from ions, electrons and defect structure within the materials. The

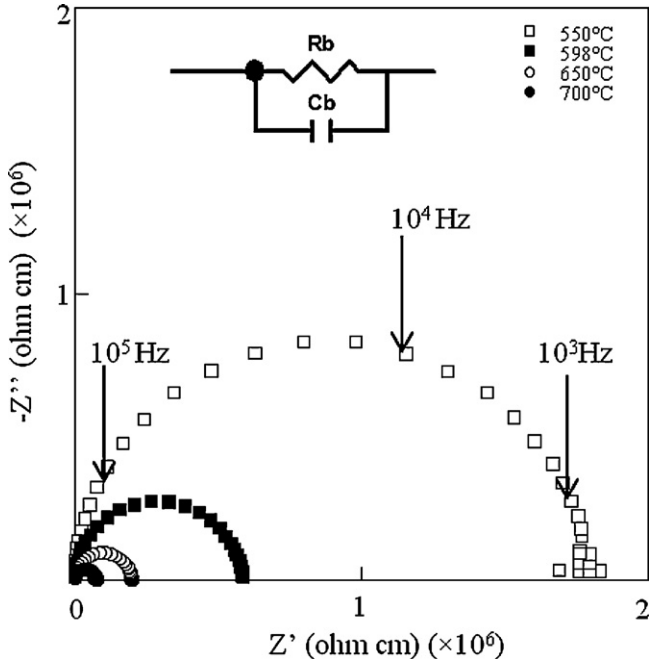

Fig. 7. Complex impedance plots of $Bi_{3.55}Mg_{1.78}Ta_{2.67}O_{13.78}$ at 550, 598, 650 and 700 °C.

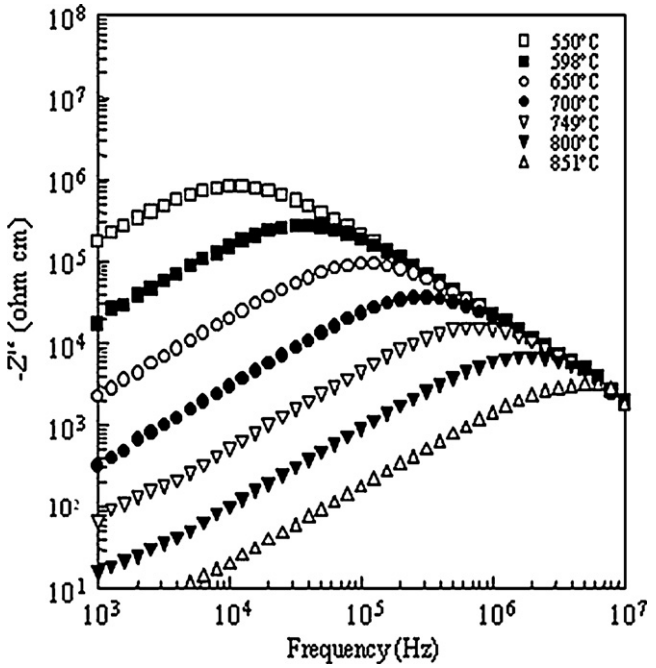

Fig. 9. Imaginary part of impedance of $Bi_{3.55}Mg_{1.78}Ta_{2.67}O_{13.78}$ as a function of frequency at different temperatures.

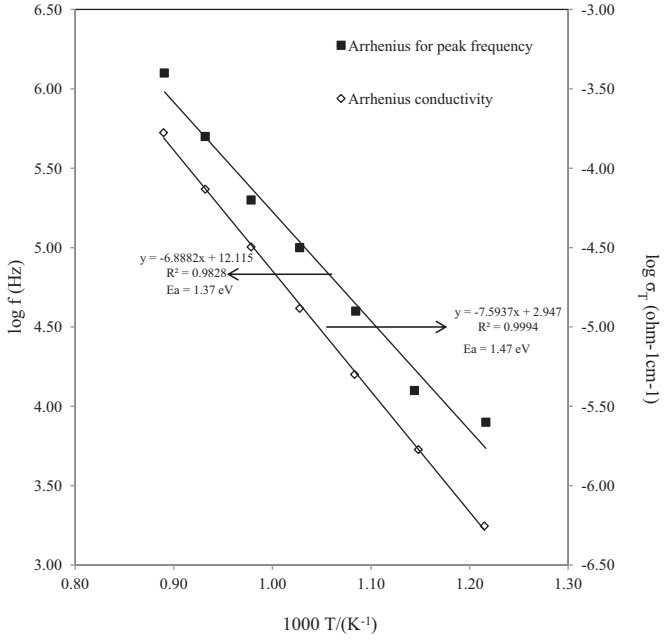

Fig. 10. Arrhenius plot for the peak frequency and the conductivity Arrhenius plot of $Bi_{3.55}Mg_{1.78}Ta_{2.67}O_{13.78}$.

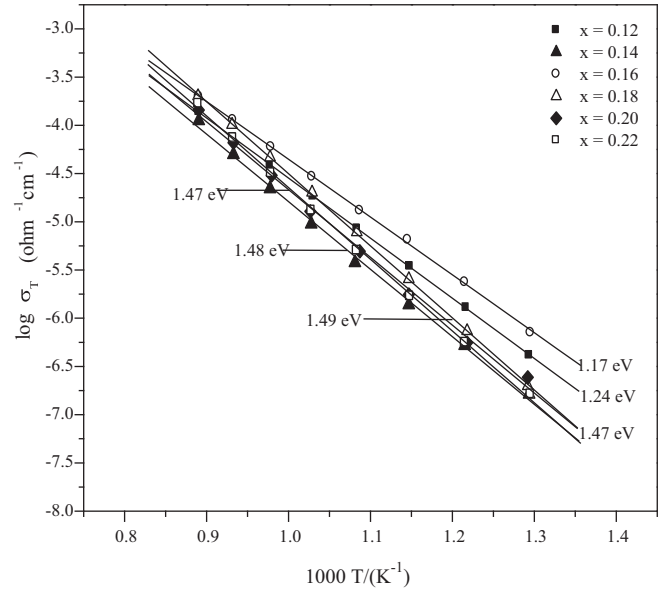

Fig. 11. The conductivity Arrhenius plots of the $Bi_{3+(5/2)x}Mg_{2-x}Ta_{3-(3/2)x}O_{14-x}$ ($0.12 \leq x \leq 0.22$) samples.

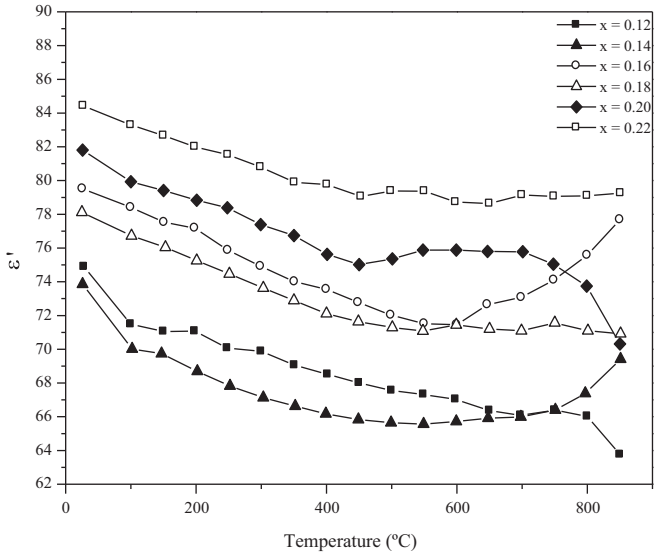

Fig. 12. The temperature dependency of the dielectric constants of prepared samples at frequency 1 MHz.

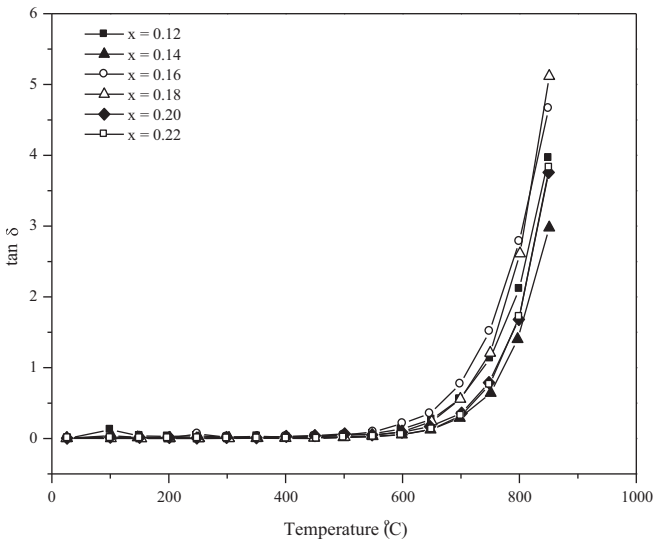

Fig. 13. The temperature dependency of the dielectric losses of the prepared samples at frequency 1 MHz.

cations occupied at different sites have different ionic radii and polarisability. The changes of the dielectric constant are influenced by the compositional variables in the materials [29]. Moreover, the high polarisability, α of Bi^{3+} ($\alpha = 6.12$ Å^3) also facilitates the polarisation process, contributing towards high dielectric constant [30]. On the other hand, dielectric losses in all samples are low and of order, 10^{-3} and this may attributed to the MgO, which serves to prevent high thermal loss during electrical conduction. The electrical properties of the samples are summarised in Table 4.

Table 4
Summary of electrical properties of $Bi_{3+(5/2)x}Mg_{2-x}Ta_{3-(3/2)x}O_{14-x}$ ($x = 0.12$–0.22) cubic pyrochlores.

Composition (x)	ε'	tan δ	TCε', ppm/°C (~30–300 °C)	E_a, eV
0.12	74	0.0026	−246	1.24
0.14	73	0.0031	−328	1.48
0.16	79	0.0044	−211	1.17
0.18	78	0.0023	−207	1.49
0.20	81	0.0059	−197	1.47
0.22	84	0.0062	−158	1.47

4. Conclusion

The pyrochlores provide great compositional variable and structural flexibility to form a wide range of solid solution in which the BMT cubic pyrochlore phases are successfully prepared with the proposed mechanism, $Bi_{3+(5/2)x}Mg_{2-x}Ta_{3-(3/2)x}O_{14-x}$ $(0.12 \leq x \leq 0.22)$. These samples have the grains sizes in the range of 0.6–10.6 μm after sintering at 1075 °C. Five infrared-active modes are observed in the subsolidus solution. All of the samples have a linear behaviour with activation energies ranging from ∼1.17 to 1.49 eV. The dielectric constants of the samples are in the range of 73–84 together with a negative temperature coefficient of permittivity, TCε'.

Acknowledgements

Special thanks for financial support from Ministry of Higher Education, Malaysia via Fundamental Research Grant Scheme (FRGS) and P.Y. Tan thanks Ministry of Science, Technology and Innovation (MOSTI) for her NSF scholarship.

References

[1] M.A. Subramanian, G. Aravamudan, G.V. Subba Rao, Oxide pyrochlore – a review, Prog. Solid St. Chem. 15 (1983) 55–143.
[2] K. Sudheendran, K.C.J. Raju, M.V. Jacob, Microwave dielectric properties of Ti-substituted $Bi_2(Zn_{2/3}Nb_{4/3})O_7$ pyrochlores at cryogenic temperatures, J. Am. Ceram. Soc. 92 (6) (2009) 1268–1271.
[3] H.J. Youn, T. Sogabe, C.A. Randall, T.R. Shrout, M.T. Lanagan, Phase relations and dielectric properties in the Bi_2O_3–ZnO–Ta_2O_5 system, J. Am. Ceram. Soc. 84 (2001) 2557–2562.
[4] C.C. Khaw, K.B. Tan, C.K. Lee, High temperature dielectric properties of cubic bismuth zinc tantalate, Ceram. Int. 35 (2009) 1473–1480.
[5] H. Wang, H. Du, Z. Peng, M. Zhang, X. Yao, Improvements of sintering and dielectric properties on Bi_2O_3–ZnO–Nb_2O_5 pyrochlore ceramics by V_2O_5 substitution, Ceram. Int. 30 (2004) 1225–1229.
[6] H. Du, X. Yao, Synthesis and dielectric properties development of new thermal stable bismuth pyrochlores, J. Phys. Chem. Solids 63 (2002) 2123–2128.
[7] C.C. Khaw, C.K. Lee, Z. Zainal, Pyrochlore phase formation in the system Bi_2O_3–ZnO–Ta_2O_5, J. Am. Ceram. Soc. 90 (6) (2007) 2900–2904.
[8] M.A.L. Nobre, S. Lanfredi, The effect of temperature on the electric conductivity property of $Bi_3Zn_2Sb_3O_{14}$ pyrochlore type phase, J. Mater. Sci.: Mater. Electron. 13 (2002) 235–238.
[9] D. Huiling, Y. Xi, Structural trends and dielectric properties of Bi-based pyrochlores, J. Mater. Sci.: Mater. Electron. 15 (2004) 613–616.
[10] H. Du, X. Yao, Evolution of structure and dielectric properties on Bismuth-based pyrochlore with TiO_2 incorporation, J. Electroceram. 9 (2002) 117–124.
[11] L.B. Kong, S. Li, T.S. Zhang, J.W. Zhai, F.Y.C. Boey, J. Ma, Electrically tunable dielectric materials and strategies to improve their performances, Prog. Mater. Sci. 55 (2010) 840–893.
[12] R.D. Shannon, Revised effective ionic radii and systematic studies of interatomic distances in halides and chalcogenides, Acta Crystallogr. Sect. A: Found. Crystallogr. 32 (1976) 751–767.
[13] D.P. Cann, C.A. Randall, T.R. Shrout, Investigation of the dielectric properties of bismuth pyrochlores, Solid State Commun. 100 (7) (1996) 529–534.
[14] V.P. Sirotinkin, A.A. Bush, Preparation and dielectric properties of $Bi_{1.5}MNb_{1.5}O_7$ (M = Cu, Mg, Mn, Ni, Zn) pyrochlore oxides, Inorg. Mater. 39 (9) (2003) 1130–1133.
[15] B. Nguyen, Y. Liu, R.L. Withers, The local crystal chemistry and dielectric properties of the cubic pyrochlore phase in the $Bi_2O_3M_2ONb_2O_5$ ($M_2 = Ni^{2+}$ and Mg^{2+}) systems, J. Solid State Chem. 180 (2007) 49–557.
[16] K.T. Jacob, S. Raj, L. Rannesh, Vegard's law: a fundamental relation or an approximation, Int. J. Mater. Res. (2007) 776–779.
[17] I. Levin, T.G. Amos, J.C. Nino, T.A. Vanderah, C.A. Randall, M.T. Lanagan, Structural study of an unusual cubic pyrochlore $Bi_{1.5}Zn_{0.92}Nb_{1.5}O_{6.92}$, J. Solid State Chem. 168 (2002) 69–75.
[18] K.B. Tan, C.C. Khaw, C.K. Lee, Z. Zainal, G.C. Miles, Structures and solid solution mechanisms of pyrochlore phases in the systems Bi_2O_3–ZnO–$(Nb,Ta)_2O_5$, J. Alloy Compd. 508 (2010) 457–462.
[19] G.C. Miles, A.R. West, Pyrochlore phases in the system ZnO–Bi_2O_3–Sb_2O_5: II. Crystal structures of $Zn_2Bi_{3.08}Sb_{2.92}O_{14+\delta}$ and $Zn_{2+x}Bi_{2.96-(x-y)}Sb_{3.04-y}O_{14.04+\delta}$, Solid State Sci. 8 (2006) 1422–1429.
[20] H. Wang, H. Du, X. Yao, Structural study of Bi_2O_3–ZnO–Nb_2O_5 based pyrochlores, Mater. Sci. Eng. B99 (2003) 20–24.
[21] K.B. Tan, C.K. Lee, Z. Zainal, C.C. Khaw, Y.P. Tan, H. Shaari, Reaction study and phase formation in Bi_2O_3–ZnO–Nb_2O_5 ternary system, J. Sci. Technol. (2008) 468–479.
[22] O.M. Lemine, Microstructural characterisation of α-Fe_2O_3 nanoparticles using, XRD line profiles analysis, FE-SEM and FT-IR, Superlattice Microstruct. 45 (2009) 576–582.
[23] R. Yogamalar, V. Mahendran, R. Srinivasan, A. Beitollahi, R.P. Kumar, A.C. Bose, A. Vinu, Gas-sensing properties of needle-shaped Ni-doped SnO_2 nanocrystals prepared by a simple sol–gel chemical precipitation method, Chem. Asian J. 5 (2010) 2379–2385.
[24] H. Du, X. Yao, L. Zhang, Structure, IR spectra and dielectric properties of Bi_2O_3–ZnO–SnO_2–Nb_2O_5 quaternary pyrochlore, Ceram. Int. 28 (2002) 231–234.
[25] M. Chen, D.B. Tanner, J.C. Nino, Infrared study of the phonon modes in bismuth pyrochlores, Phys. Rev. B 72 (2005) 054303.
[26] H. Du, X. Yao, Dielectric relaxation characteristics of bismuth zinc niobate pyrochlores containing titanium, Phys. B: Condens. Matter 324 (2002) 121–126.
[27] H. Du, X. Yao, X. Zhang, H. Weng, Defect structure and dielectric properties of Bi-based pyrochlores probed by positron annihilation, Appl. Surf. Sci. 253 (2006) 1856–1860.
[28] M.A. Nobre, S. Lanfredi, Dielectric spectroscopy on $Bi_3Zn_2Sb_3O_{14}$ ceramic: an approach based on the complex impedance, J. Phys. Chem. Solids 64 (2003) 2457–2464.
[29] H. Du, H. Wang, X. Yao, Observations on structural evolution and dielectric properties of oxygen-deficient pyrochlores, Ceram. Int. 30 (2004) 1383–1387.
[30] R.D. Shannon, Dielectric polarizabilities of ions in oxides and fluorides, J. Appl. Phys. 73 (1) (1993) 348–366.